JGR: Space Physics

Supporting Information for

Advancing our Understanding of Martian Proton Aurora through a Coordinated Multi-Model Comparison Campaign

Andréa C. G. Hughes[1,2,3], Michael Chaffin[4], Edwin Mierkiewicz[3], Justin Deighan[4], Rebecca D. Jolitz[4], Esa Kallio[5], Guillaume Gronoff[6,7], Valery Shematovich[8], Dmitry Bisikalo[8,9], Jasper Halekas[10], Cyril Simon Wedlund[11], Nicholas Schneider[4], Birgit Ritter[12,13], Zachary Girazian[10], Sonal Jain[4], Jean-Claude Gérard[12], and Bradley Hegyi[6,7]

[1] NASA Goddard Space Flight Center, Greenbelt, MD, United States.
[2] Department of Physics & Astronomy, Howard University, Washington, DC, United States.
[3] Center for Space and Atmospheric Research (CSAR) and the Department of Physical Sciences, Embry-Riddle Aeronautical University, Daytona Beach, Florida, United States.
[4] Laboratory for Atmospheric and Space Physics, University of Colorado, Boulder, CO, USA. United States.
[5] Aalto University, School of Electrical Engineering, Department of Electronics and Nanoengineering, Espoo, Finland.
[6] NASA Langley Research Center, Hampton, VA, United States.
[7] Science Systems and Application Inc. Hampton, VA, United States.
[8] Institute of Astronomy of the Russian Academy of Sciences, Moscow, Russia.
[9] National Center for Physics and Mathematics, Russian Federation, Moscow, Russia.
[10] Department of Physics and Astronomy, University of Iowa, Iowa City, IA, United States.
[11] Space Research Institute, Austrian Academy of Sciences, Graz, Austria.
[12] Royal Observatory of Belgium, Brussels, Belgium.
[13] Université de Liège, LPAP – STAR Institute, Liege, Belgium.

Contents of this file

Text S1 to S4
Figures S1 to S4
Tables S1 to S1

Introduction

Herein we provide supplemental materials regarding the models used in the study, cross sections used in the models, and additional information regarding the locations of MAVEN and MAVEN/IUVS for observations taken during the orbit of interest. In the Supplementary Text section, we present detailed descriptions of each of the four proton/hydrogen precipitation models used in the study. Descriptions are written by each modeling team and appropriate references are given at the end of each section. In the Supplementary Figures section, we present S1) maps showing the locations of the MAVEN spacecraft during the orbit used in this study (including comparative locations of strong crustal fields), S2) ephemeris data for the MAVEN/IUVS instrument while acquiring the periapsis limb scan data used in this study, S3) relevant profiles used for the coronal thermal H background subtraction method described in the text, and S4) preliminary results comparing the assumption of monodirectional incident particle movement versus isotropic. Lastly, we include a Supplementary Table with details regarding cross sections used by each model and relevant references.

Text S1.

Kallio 3-D Monte Carlo Model Description

(i) General introduction: nature of the model, brief history of its development, and general references

The Kallio model is described in detail in *Kallio and Barabash*, 2000 and 2001. The model is a 3-D Monte Carlo (MC) model where the incident particle, either H^+ or H, collides with neutral particles after which the velocity of the particle is changed. The model contains 6 elastic and 24 inelastic processes but, in this study, only the processes mentioned in the main text of this paper were used.

The model uses a Cartesian coordinate system both for the positions and velocities of the precipitating particles. In the coordinate system the x-axis points from the center of Mars toward the Sun.

(ii) Inputs, processes included (with relevant cross section references), and outputs

The model inputs are neutral atom densities, energy dependent total cross-sections (CS), the differential scattering cross-sections (DSCS), the number of precipitating particles (N_H), and the initial positions ($\boldsymbol{r}_{\mathrm{particle}}(t=0)$) and velocities ($\boldsymbol{v}_{\mathrm{particle}}(t=0)$) of the precipitating particles -- in the present case hydrogen atoms (H).

The total cross sections are given in *Kallio and Barabash, 2001* (Table 1 and Fig. 3) and the DSCS scattering angle distribution in *Kallio and Barabash*, 2000 (Fig. 1, “nominal”) and 2001 (Fig. 2). Total cross sections give the probability that a collision occurs. Random numbers are used to model if a collision occurs, and which collision process occurs. If a collision happens, then the DSCS determines the new velocity of the incident particle after collision. The value of the scattering angle is obtained by using a new random variable.

(iii) Implementation and technical aspects: assumptions and constraints, domain of applicability and grid description, spatial resolution and timesteps, number of particles, overall performance, etc.

In the simulation, particles are injected into the upper atmosphere at the point [x, y, z] = [260 km + R_{Mars}, 0, 0], where the radius of the Mars, R_{Mars}, was in the simulation 3393 km. The velocity of the particles in the analysis presented in this paper was a constant $\boldsymbol{v} = [v_x, v_y, v_z] = [-400, 0,0]$ km/s, i.e., a beam of particles initially moving exactly along the Sun-Mars line.

The model saves the position and the velocity of the particle if it has a Ly-α collision process. The Ly-α volume production rate was derived from the saved positions of Ly-α processes by collecting the number of the Ly-α collision processes ($\mathrm{d}\#_k^{hf}$) at a given altitude (h) range: $\mathrm{d}h_k \equiv h_{k+1} - \mathrm{d}h_k$. Then in Step 1 runs the Ly-α volume of the emission was derived by using a 1-D approximation, i.e., assuming that the area of the emission perpendicular to the x-axis ($\mathrm{d}A_{hf}$) is equal to the initial area in the solar wind ($\mathrm{d}A_{sw}$) through which the precipitating particles initially came, $\mathrm{d}A_{hf} = \mathrm{d}A_{sw}$. Note that the inaccuracy caused by the 1-D approximation, $\mathrm{d}A_{hf} = \mathrm{d}A_{sw}$, is small because the horizontal movement of the colliding particles in the atmosphere is small compared with the radius of the planet. Therefore, the volume ($\mathrm{d}V_k$) from which the emission came within $\mathrm{d}h_k$ in Step 1 runs was assumed to be $\mathrm{d}V_k = \mathrm{d}h_k \times \mathrm{d}A_{sw}$. In Step 2 runs the volume $\mathrm{d}V_k$ was derived without any approximations from the space angle and the altitude range.

The altitude dependent Ly-α volume emission rate

$$q_k^{hf} = \mathrm{d}\#_k^{hf} / (\mathrm{d}t \times \mathrm{d}V_k) = \mathrm{d}\#_k^{hf} / (\mathrm{d}t \times \mathrm{d}h_k \times \mathrm{d}A_{hf}), \quad (1)$$

which, as mentioned above, was in Step 1 runs derived by approximating $\mathrm{d}A_{hf} = \mathrm{d}A_{sw}$

$$q_k^{hf} = \mathrm{d}\#_k^{hf} / (\mathrm{d}t \times \mathrm{d}h_k \times \mathrm{d}A_{sw}), \quad (2)$$

is finally obtained from the particle flux of the precipitating H particles (j_H), the number of the particles used in the MC simulation (N_H) and the time ($\mathrm{d}t$) which takes N_H particles to go through the area $\mathrm{d}A_{sw}$: $N_H = j_H\ \mathrm{d}t \times \mathrm{d}A_{sw}$. This gives $\mathrm{d}t \times \mathrm{d}A_{sw} = N_H / j_H$ and Eq (2) gets the form

$$q_k^{hf} = \mathrm{d}\#_k^{hf} / (\mathrm{d}t \times \mathrm{d}V_k) = j_H\ [\mathrm{d}\#_k^{hf} / (\mathrm{d}h_k \times N_H)]. \quad (3)$$

In the analyzed simulation N_H was 5000 and 100,000 in Step 1 and Step 2 runs, respectively. As can be seen in Eq. (3) the particle flux j_H is just a scaling factor and in this paper, it was 10^7 cm^{-3} s^{-1}. In the plots presented in this paper the Ly-α emission altitude profiles were derived in 1 km altitude bins, i.e., $\mathrm{d}h_k = 1$ km. This provided a relatively good compromise between modest statistical fluctuations and the accurate determination of the peak emission value and altitude.

(iv) Strengths and applications most suited for the model

The largest uncertainty for the obtained Ly-α volume emission rate q_k^{hf} is related to the uncertainty of the total cross-sections used and the differential scattering cross sections between H and H^+ particles and CO_2 molecules. In the simulation many of these

H/H^+ collisions with CO_2 are modeled with H/H^+ collisions with O_2 and N_2 which was published in the literature (see *Kallio and Barabash*, 2001, Table 1, for details).

As described in *Kallio and Barabash*, 2000 and 2001, functional forms of the adopted DSCS are modeled following *Noël and Prölss* (1993). The used DSCS (see *Kallio and Barabash*, 2000, Fig. 1a, the "nominal" DCSC and *Kallio and Barabash*, 2001, Fig. 2) is a fit to the data of H – O_2 collisions from *Newmann et al*., 1986, Table 4.

It is worth noting that although the statistical fluctuations in the derived emission altitude profiles could be reduced by using a larger number of precipitating particles in the 1 km altitude binning used, the statistical fluctuations are relatively modest already for the number of particles used.

It is also worth noting that the MC model used can be automatically used in future more complicated situations than done in this paper. In this study the precipitating particles formed a monoenergetic beam. However, the velocity distribution function can be more complicated; for example, a Maxwellian velocity distribution function, or the velocities can be read from a file. Moreover, the atmospheric density profile, $n(\boldsymbol{r})$ can be 2-D, say $n(\boldsymbol{r}) = n(\mathrm{SZA}, h)$. In such a case the MC model can be used to derive altitude profiles at a given SZA (see *Kallio and Barabash*, 2001, for details). The atmospheric density can also be 3-D, i.e., $n(\boldsymbol{r}) = n(\mathrm{x, y, z})$, which would result in the 3-D Ly-α emission rates. In the simulation the particle flux and their velocity distribution can also have latitude-longitude dependence (see *Kallio and Janhunen*, 2001, for details).

References:

Kallio, E., and S. Barabash, On the elastic and inelastic collisions between precipitating energetic hydrogen atoms and Martian atmospheric neutrals J. Geophys. Res., 105, 24,973-24,996, 2000.

Kallio, E., and S. Barabash, Atmospheric effects of precipitating energetic hydrogen atoms on the Martian atmosphere, J. Geophys. Res., 106, 165-178, 2001.

Kallio, E., and P. Janhunen, Atmospheric effects of proton precipitation in the Martian atmosphere and its connection to the Mars-solar wind interaction, J. Geophys. Res., 106, 5617-5634, 2001.

Newman, J. H., Y. S. Chen, K. A. Smith and R. F. Stebbings, Differential cross sections for scattering of 0.5-, 1.5-, and 5.0-keV hydrogen atoms by He, H2, N2, and O2, J. Geophys. Res., Volume 91, Issue A8, Pages 8947-8954,1986.

Noël, S. and G. W. Prölss, Heating and radiation production by neutralized ring current particles. J. Geophys. Res., Volume 98, Issue A10, Pages 17317-17325,1993.

Rees, M. H., Physics and Chemistry of the Upper Atmosphere, Cambridge Univ. Press, New York, 1989.

Rudd, M. E., Kim, Y. K., Madison, D. H., & Gallagher, J. W., Electron production in proton collisions: Total cross sections. Reviews of Modern Physics, 57, 965– 994, 1985.

Van Zyl, B., Neumann, H., Le, T. Q., and R.C. Amme, H + N2 and H + O2 collisions: Experimental charge-production cross sections and differential scattering calculations, Phys. Rev. A 18(2):506-516, 1978.

Van Zyl, B., and H. Neumann, Lyman α emission cross sections for low-energy H and H+ collisions with N2 and O2, J. Geophys. Res, 93(A2):1023-1027, 1988.

Text S2.

Jolitz 3-D Monte Carlo Model Description (Name: "ASPEN")

ASPEN (Atmospheric Scattering of Protons, Electrons, and Neutrals) is a 3-D Monte Carlo test particle simulation. This model was initially developed to predict atmospheric ionization rates at Mars by solar energetic particles, which have higher energies than the ENAs studied in this paper [Jolitz *et al.*, 2017] and has since been used to predict precipitating SEP electron fluxes at Mars [Jolitz *et al.*, *2021*]. The simulation solves the Lorentz force equations for energetic particle motion and uses a Monte Carlo approach to predict collisions and resulting energy loss in the atmosphere. Since magnetic fields were set to zero for this study, the transport equations reduced to ballistic motion.

The collisional energy degradation algorithm used in ASPEN was originally developed and described in Lillis *et al.* [2008] for an electron precipitation model. It is very similar to the Kallio model in approach. Stochastic collisions were modeled by inverting the relation between intensity, density, and absorption cross-section for a particle beam incident on a medium of scatterers (colloquially known as Beer's law) to dynamically calculate a probability distribution function that is combined with a random number to predict variable distances between collisions. This probability distribution function is calculated for each individual particle and depends on the position, path, and energy through the planetary atmosphere. Similarly, whenever a collision occurs, the type of collision is predicted probabilistically using the relative cross-section of each possible collisional process and the particle energy is decremented by the corresponding energy loss. As a particle loses energy, the relative cross-sections of each process change. For example, a 2 keV proton colliding with a carbon dioxide molecule has a roughly 70% likelihood of capturing an electron, but the likelihood for the same process when the proton is 20 eV is only 20%.

This model is highly dependent on the choice of cross-sections. For the application in this study, the selected cross-sections for hydrogen and proton impact on carbon dioxide are described in Jolitz *et al.* [2017], with one exception. The cross-sections for proton- and hydrogen-impact excitation was replaced with Lyman-alpha emission cross-sections. Unfortunately, experimental measurements of the Lyman-alpha emission cross-section from proton and hydrogen atom impact on carbon dioxide is limited. As of the time of this paper's writing, only one set of measurements exist for 1-25 keV protons and hydrogen atoms [Birely and McNeal, 1972]. The cross-section for emission by protons and hydrogen atoms below 1 keV is unknown. In order to approximate emission from particles at these energies, ASPEN uses a cross-section calculated by scaling the corresponding emission cross-sections from impact on molecular oxygen. ASPEN also accounts for the fact that proton-induced Lyman-alpha emission can only occur in addition to a charge exchange collision, since Lyman-alpha can only be emitted by a hydrogen atom.

Since ASPEN is a 3-D Monte Carlo simulation, predicting an accurate emission rate requires appropriate choice of initial conditions and a large volume of simulated particles. For Step 1, we simulated 10,000 particles incident on the subsolar point from an altitude of 600 km and calculated the emission rate by binning all Lyman-alpha emitting collisions as a function of altitude and multiplying by the incident flux. For Step 2, we simulated 10,000 particles uniformly distributed in space on a plane perpendicular to the direction of solar wind flow. Each particle represents a fraction of the assumed incident flux. The emission rate was then calculated by weighing the total number of emissions binned by altitude, solar zenith angle, and the fraction of flux associated with each simulated particle.

References:

Avakyan, S. V., R. N. Il'in, V. M. Lavrov, and G. N. Ogurtsiv (1998), Collision Processes and Excitation of UV Emission From Planetary Atmospheric Gases: A Handbook of Cross Sections, Gordon and Breach, Amsterdam.

Barnett, C. F., Ray J. A., Ricci, E., Wilkers, M. I., et al. 1977. Atomic data for controlled fusion research. Report no. ORNL-5296. Oak Ridge, TN: Oak Ridge National Laboratory.

Birely, J.H., and R.J. McNeal (1972), Lyman-alpha emission cross sections for collisions of 1-25 keV H+ and H with CO, CO2, CH4, and NH3, J.Chem Phys., 56 (5), 2189-94, doi:10.1063/1.1677518.

Jolitz, R. D., C. F. Dong, C. O. Lee, R. J. Lillis, D. A. Brain, S. M. Curry, S. Bougher, C. D. Parkinson, and B. M. Jakosky (2017), A Monte Carlo model of crustal field influences on solar energetic particle precipitation into the Martian atmosphere, J. Geophys. Res. Space Physics, 122, 5653–5669, doi:10.1002/2016JA023781.

Jolitz, R. D., Dong, C. F., Rahmati, A., Brain, D. A., Lee, C. O., Lillis, R. J., Curry, and B. M. Jakosky (2021). Test particle model predictions of SEP electron transport and precipitation at Mars. *Journal of Geophysical Research: Space Physics*, 126, e2021JA029132. https://doi. org/10.1029/2021JA029132

Lillis, R. J., D. L. Mitchell, R. P. Lin, and M. H. Acuña (2008), Electron reflectometry in the Martian atmosphere, Icarus, 194(2) 544-61, doi:10.1016/j.icarus.2007.09.030.

McNeal, R.J. (1970), Production of positive ions and electrons in collisions of 1-25-keV protons and hydrogen atoms with CO, CO2, CH4, and NH3, J. Chem. Phys. 53, 4308.

Nakai, Y., T. Shirai, T. Tabata, and R. Ito (1987), Cross sections for charge transfer of hydrogen atoms and ions colliding with gaseous atoms and molecules, At. Data Nucl. Data Tables, 37, 69– 101, doi:10.1016/0092-640X(87)90005-2.

Newman, J. H., Chen, Y.S., Smith, K.A., and R.F. Stebbings (1986), Differential cross sections for scattering of 0.5-, 1.5-, and 5.0-keV hydrogen atoms by He, H2, N2, and O2, J. Geophys. Res. 91(A8), 8947–8954.

Noël S., and G. W. Prölss (1993), Heating and radiation production by neutralized ring current particles. J Geophys Res 98:17317–17325.

Rudd, M. E., Kim, Y. K., Madison, D. H., & Gallagher, J. W. (1985), Electron production in proton collisions: Total cross sections. Reviews of Modern Physics, 57, 965– 994.

Van Zyl, B., Neumann, H., Le, T. Q., and R.C. Amme (1978), H + N2 and H + O2 collisions: Experimental charge-production cross sections and differential scattering calculations, Phys. Rev. A 18(2):506-516.

Van Zyl, B., and H. Neumann (1988), Lyman α emission cross sections for low-energy H and H+ collisions with N2 and O2, J. Geophys. Res, 93(A2):1023-1027.

Text S3.

Bisikalo/Shematovich *et al.* 1-D Monte Carlo Model Description

The Bisikalo/Shematovich et al. model is a 1-D kinetic Monte Carlo model. The model considers three primary processes: 1) precipitation of high-energy hydrogen atoms and protons that lose their kinetic energy in the elastic and inelastic collisions, 2) ionization of target atmospheric molecules/atoms, and 3) charge transfer and electron capture collisions with the major atmospheric constituents (i.e., CO2, N2, and O). Secondary fast hydrogen atoms and protons carry enough kinetic energy to cycle through the collisional channels mentioned above and result in a growing set of translationally and internally excited atmospheric atoms and/or molecules.

To study the precipitation of high-energy H/H^+ flux into the planetary atmosphere, we solve the kinetic Boltzmann equations (Shematovich *et al.*, 2011) for H^+ and H, including the collision term:

$$\mathbf{v}\frac{\partial}{\partial \mathbf{r}} f_{H/H+} + \left(\mathbf{g} + \frac{e}{m_{H+}}\mathbf{v}\times\mathbf{B}\right)\frac{\partial}{\partial \mathbf{v}} f_{H/H+} = Q_{H/H+}(\mathbf{v}) + \sum_{M=O,N_2,CO_2} J_{mt}(f_{H/H+}, f_M). \quad (1)$$

Equation (1) is written in the standard form for the velocity distribution functions $f_{H/H+}(r,v)$, and $f_M(r,v)$ for hydrogen atoms and protons (Gérard *et al.*, 2000). The source term $Q_{H/H+}$ describes the production rate of secondary H/H^+ particles and the elastic and inelastic collisional terms J_{mt} for H/H^+ describe the energy and momentum transfer to the ambient atmospheric gas which is characterized by local Maxwellian velocity distribution functions. Our kinetic Monte Carlo model (Gérard *et al.*, 2000; Shematovich *et al.*, 2011) is used to solve kinetic equation (1). The model is 1-D in geometric space and 3-D in velocity space. Nevertheless, the 3-D trajectories of H/H^+ are calculated in the code with final projection on radial direction. In the current version of the MC model (Shematovich *et al.*, 2019) an arbitrary structure of the induced magnetic field of Mars is included; that is, all three components of the magnetic field **B** = $\{Bx,By,Bz\}$, were taken into account. The details of the model implementation and statistics control with the variance below 10% can be found in (Shematovich *et al.*, 2019).

The essence of the kinetic Monte Carlo model is accounting of all possible collisions in the atmospheric region studied. Therefore, statistics for all collisional processes are accumulated during the numerical realization of the kinetic model of the proton aurora. It provides a good basis for the evaluation of the Ly-α source functions as keeping of all excitation processes and their spatial characteristics makes it possible to determine the statistical distribution of the emitted Ly-α photons.

The energy deposition rate of H/H+ flux is determined by the cross sections of the collisions with the ambient gas. The energy lost by the H/H+ in a collision is determined by the scattering angle χ

$$\Delta E \sim E \times (1 - cos\chi),$$

where E is the initial energy of the impacting proton or hydrogen atom. It is apparent that the energy loss for collisions in forward direction (for $\chi < 90°$) at small scattering angles χ is less than that for larger scattering angles. A key aspect of this kinetic MC model is the probabilistic treatment of the scattering angle distribution, which influences both the energy degradation rate and the angular redistribution of the precipitating protons and hydrogen atoms (Bisikalo et al., 2018; Shematovich et al., 2019). The kinetic model utilizes both total and differential cross sections when calculating the post-collision velocities for high-energy precipitating H/H+ and atmospheric particles. In the model, the most recent measurements or calculations of the required cross sections were adopted. The cross sections and scattering angle distributions for H/H+ collisions with CO2 are taken from Nakai et al. (1987) for charge exchange and stripping collisions, from Haider et al. (2002) for ionization, Lyman alpha and Balmer alpha excitation, and from Lindsay et al. (2005) for scattering angle distributions. The elastic and other inelastic collisions cross sections for H/H+ collisions with CO2 are assumed to be the same as for O2 (see, for details, Gérard et al. (2000)). The region under study is limited by the lower boundary, which is placed at 80 km, where H/H^+ particles are efficiently thermalized. The upper boundary is set at 500 km, where measurements or calculations of the precipitating fluxes of protons or hydrogen atoms are used as a boundary condition. Both table and/or analytic (Maxwellian and/or kappa-distribution) functions representing the energy spectra as well as the pitch-angle (monodirectional, isotropic, or limited by cone) distributions of precipitating particles could be used at the upper boundary. Detailed description of all modeled numerical aspects used for this kinetic MC model study could be found in recent papers (Bisikalo *et al.*, 2018; Shematovich *et al.*, 2019).

References:

Gérard J.-C., Hubert B., Bisikalo D.V., and Shematovich V.I. Lyman-alpha emission in the proton aurora. J. Geophys. Res., 2000, V. 105, No. A7, pp. 15795.

Shematovich V. I., D. V. Bisikalo, C. Diéval, S. Barabash, G. Stenberg, H. Nilsson, Y. Futaana, M. Holmstrom, and J.-C. Gérard. Proton and hydrogen atom transport in the Martian upper atmosphere with an induced magnetic field. J. Geophys. Res., 2011, V. 116, Issue A11, CiteID A11320.

Bisikalo D.V., Shematovich V.I., Gérard J.-C., Hubert B. Monte Carlo simulations of the interaction of fast proton and hydrogen atoms with the Martian atmosphere and comparison with in situ measurements. Journal of Geophysical Research: Space Physics, 2018, V. 123, Issue 7, pp. 5850-5861.

Shematovich V.I., Bisikalo D.V., Gérard J.-C., Hubert B. Kinetic Monte Carlo model of the precipitation of high-energy proton and hydrogen atoms into the Martian atmosphere with taking into account the measured magnetic field. Astronomy Reports, 2019, Vol. 63, No. 10, pp. 835–845.

Haider, S.A., Seth S. P., Kallio E., and Oyama K.I. Solar EUV and electron-proton-hydrogen atom-produced ionosphere on Mars: Comparative studies of particle fluxes and ion production rates due to different processes, Icarus, 2002, V. 159, pp. 18-30.

Lindsay, B. G., Yu W. S., and Stebbings R. F. Cross sections for electron capture and loss by keV oxygen atoms in collisions with CO and CO2, J. Geophys. Res., 2005, V. 110, pp. A02302.

Nakai, Y., Shirai T., Tabata T., and Ito R. Cross sections for charge transfer of hydrogen atoms and ions colliding with gaseous atoms and molecules, Atomic Data and Nuclear Data Tables, 1987, V.37, pp. 69-101.

Text S4.

Gronoff *et al.* 1-D Kinetic Model Description (Name: "Aeroplanets")

A. Introduction

The *Aeroplanets* model (Gronoff *et al.,* 2012a; Gronoff *et al.,* 2012b; Simon Wedlund *et al.* 2011) is a 1-D kinetic transport model computing the ionization and excitation of atmospheric species by photon, electron, proton, and cosmic ray impacts, including the effect of secondary particles (photoelectrons, secondary electrons and protoelectrons). It is based on the Trans* model series, initially developed for the Earth (Lilensten *et al.,* 1999; Lummerzheim and Lilensten 1994; Simon *et al.,* 2007 as Trans4), and subsequently adapted to Venus (Gronoff *et al.,* 2007, 2008), Mars (Witasse *et al.,* 2002, 2003; Simon *et al.,* 2009; Nicholson *et al.,* 2009), Titan (Gronoff, Lilensten, and Modolo 2009; Gronoff *et al.,* 2009a, 2009b), etc., and including several other modules such as a fluid model. Aeroplanets constitutes an improvement in modularity and adaptability over Trans4, with every separate module having the option of being turned off to study one specific aspect of particle precipitation in the atmosphere of planets.

The proton transport module is based on the work of Galand *et al.* (1997, 1998), Simon (2006) and Simon *et al.* (2007) for Earth, who solved semi-analytically the coupled proton-hydrogen dissipative kinetic transport equation for protons and hydrogen atoms charge-changing with neutral gas M:

$H^+ + M \rightarrow H + M^+ Electron\ capture, \sigma_{10}$ $H + M \rightarrow H^+ + M + e^- Electron\ loss/stripping, \sigma_{01}$.

It naturally includes angular redistributions due to magnetic mirror effects and to collisions (Galand *et al*., 1998)

B. Inputs and outputs

Inputs to the Aeroplanets model include cross sections, the vertical profile of atmosphere composition (*i.e.*, composition at different altitudes), and the precipitating fluxes of particles such H and H^+ at the top of the atmosphere. Outputs include the vertical profile of H and H^+ differential energy fluxes, and the vertical profile of the production rate of excited and ionized species and electrons, including emissions. The produced photoelectrons can be plugged into the main Aeroplanets electron model as an external and additional source of ionization in the atmosphere.

Cross sections in Aeroplanets are taken from the latest version of the ATMOCIAD cross section and reaction rate database compiled and developed by Simon Wedlund *et al.* (2011), Gronoff *et al.* (2012a) and Gronoff *et al.* (2020), and freely available in Gronoff et al. (2021) In ATMOCIAD, experimental and theoretical cross sections as well as their uncertainties are collected. Many proton-hydrogen impact cross sections have been discussed in the seminal works of Avakyan *et al.* (1998) and, in a lesser degree, of Nakai *et al. (*1987); they contain a critical review of processes for photons, e^-, H, H^+ colliding with various gases of aeronomic interest and have been fully integrated into ATMOCIAD.

Specifically, the proton transport code uses the following energy-dependent cross sections, process by process:

- **Elastic**. Parameterisations of Kozelov and Ivanov (1992) originally valid for (H^+, H) collisions with N_2, and assumed to be the same for CO_2 because of the lack of any recent measurements. The parameters are available in their Tables 1 and 2.
- **Ionization**. For H^+, Rudd *et al.* (1983) for high energies, extended at $E < 5$ keV by (Avakyan *et al.*, 1998). For H atoms, cross sections are based on Basu *et al.* (1987) for N_2 and on Avakyan *et al.* (1998) for the rescaling factor.
- **Electron capture ($H^+ \rightarrow H$)**. Kusakabe *et al.* (2000) for 0.2-4 keV protons, review by Avakyan *et al.* (1998) based on all other available data for higher energies (Desesquelles, Do Cao, and Dufay 1966; Barnett and Gilbody 1968; Toburen, Nakai, and Langley 1968; McNeal 1970; Rudd *et al.*, 1983 for $5 - 150$ keV). Note that recent sub-keV measurements have been made by Werbowy and Pranszke (2016) for CO and CO_2, although these are not yet implemented in the ATMOCIAD.
- **Electron loss ($H \rightarrow H^+$)**. Smith *et al.*, (1976) between $0.25 - 5$ keV, review by Avakyan *et al.*, (1998) using N_2 σ_{01} cross sections (Green and Peterson 1968) based on all other available data for higher energies.
- **Ly-α H(2p) and H(2s) states**. For both H^+ and H collisions, exciting state H($2p$) (Birely and McNeal 1972) corrected by factor 0.9 presumably because of observation angle issues as per the recommendation of Avakyan *et al.* (1998). For both impactors creating state H($2s$), factor 1.35 on the measurements of (Birely and McNeal 1972) is applied.

Although ATMOCIAD is an extensive collection of cross sections, there is still a rather poor characterization of cross sections at low energies (typically in the sub-keV range).

Regarding differential cross sections, Aeroplanets uses phase functions that are convolved with the energy-dependent cross sections above. For the particular cases computed for Step 1 of the present study, the following is used: for the two charge-transfer (10 and 01) and elastic cross sections, the screened Rutherford function is used, equal to that of the electrons with a screening parameter ϵ of 10^{-3} (this is the same as in Galand *et al.*, 1997, 1998 and Simon 2006, Simon *et al.*, 2007 for Earth's atmosphere):

$$\xi(cos\vartheta) = \frac{4\epsilon(1+\epsilon)}{(1+2\epsilon - cos\vartheta)^2}$$

with $\vartheta = \mu\mu' + \sqrt{1-\mu'^2}\sqrt{1-\mu^2}cos(\phi - \phi')$. μ and μ' are the cosine of the pitch angles before and after the collision, whereas ϕ and ϕ' are the azimuthal angles before and after the collision. For ionization, forward scattering is assumed following Galand *et al.*, (1998) for the Earth case.

Because of the seamless implementation of ATMOCIAD as input to Aeroplanets, other available sets of cross sections may be used. It is possible to estimate the uncertainties from the cross sections using a Monte-Carlo approach as described in (Gronoff *et al.,* 2012a; Gronoff *et al.,* 2012b). The outputs of the proton-transport model are the ionization and dissociation rates (including excited states productions), the proton/H induced electron flux (which can be used in the electron model), and the proton/H fluxes at the different altitudes.

C. Implementation

The solution of the dissipative coupled Boltzmann H/H^{+} equation is based on the seminal work of Galand *et al.,* (1997, 1998), later developed and adapted as a module into Aeroplanets following Simon *et al.,* (2007). It is based on the idea that dissipative forces responsible for angular redistributions (due to elastic scattering) can be introduced in the force term of the generalized Boltzmann equation (Galand *et al.,* 1997). Rearranging the energy/angle terms of the H^{+}/H coupled system of equations leads to a linear system of equations parametrized by a large sparse square matrix A containing the energy degradation without angular redistributions of the incoming particle, for each altitude z so that:

$$\frac{\partial \Phi}{\partial z} = A\Phi + B$$

$\Phi = (\phi_{H^+}\ \phi_H\ )$ is the vector-flux of protons and hydrogen precipitating particles and B, the angular degradation term, is thus the term coupling downward and upward fluxes. Moreover, the mirror mode term can be switched on or off depending on the planet's configuration. The equation can be solved by calculating the exponential of matrix A for a typical grid of 100 energies and 10 angles, both of which can be increased by the user for better resolution.

In order to achieve such a feat of simplification for a complex system of equations, the following assumptions are made in the case of the Mars code: (i) plane parallel geometry, with the atmosphere stratified horizontally, and the pitch angle of the particles can be imposed, (ii) external forces neglected, (iii) steady-state fluxes, (iv) continuous slowing down approximation assumed because of the low energetic losses by the precipitating particles compared to the incident energy of the particles.

D. Strengths and applications

Aeroplanets is better qualified for the fast computation of the proton precipitation from a measured spectra near the planet, and for the fast computation of the whole effect of that precipitation thanks to its coupling with a secondary electron transport model. The analytic computation approach and assumed geometry prevent the computation within very complex magnetic topologies (which are best handled by Monte-Carlo models) but is well suited for handling large sets of initial angles and energies.

References:

Avakyan, S.V., R.N. Ii'In, V.M. Lavrov, and G.N. Ogurtsov. 1998. Collision processes and excitation of UV emission from planetary atmospheric gases: a handbook of cross sections. Taylor & Francis, Amsterdam.

Barnett, C. F., and H. B. Gilbody. 1968. "Measurements of Atomic Cross Sections in Static Gases." In Atomic Interactions Part a, edited by Benjamin Bederson and Wade L. Fite, 7:390.

Basu, B., J. R. Jasperse, R. M. Robinson, R. R. Vondrak, and D. S. Evans. 1987. “Linear transport theory of auroral proton precipitation: A comparison with observations.” J. Geophys. Res. 92 (A6): 5920–32. https://doi.org/10.1029/JA092iA06p05920.

Birely, J. H., and R. J. McNeal. 1972. “Lyman-Alpha Emission Cross Sections for Collisions of 1-25 keV H^+ and H with CO, CO_2, CH_4, and NH_3.” J. Chem. Phys. 56 (5): 2189–94. https://doi.org/10.1063/1.1677518.

Desesquelles, J., G. Do Cao, and M. Dufay. 1966. “Etude de l’ionisation de quelques gaz par des ions accélérés H^+ et H_2^+.” C. R. Acad. Sci. Paris 262 (B): 1329–32.

Galand, M., J. Lilensten, W. Kofman, and D. Lummerzheim. 1998. “Proton transport model in the ionosphere. 2. Influence of magnetic mirroring and collisions on the angular redistribution in a proton beam.” Annales Geophysicae 16 (October): 1308–21. https://doi.org/10.1007/s00585-998-1308-y.

Galand, M., J. Lilensten, W. Kofman, and R. B. Sidje. 1997. “Proton transport model in the ionosphere 1. Multistream approach of the transport equations.” Journal of Geophysics Research 102 (September): 22261–72. https://doi.org/10.1029/97JA01903.

Green, A. E. S., and L. R. Peterson. 1968. “Energy loss functions for electrons and protons in planetary gases.” J. Geophys. Res. 73 (1): 233. https://doi.org/10.1029/JA073i001p00233.

Gronoff, G., J. Lilensten, C. Simon, O. Witasse, R. Thissen, O. Dutuit, and C. Alcaraz. 2007. “Modelling Dications in the Diurnal Ionosphere of Venus.” Astronomy and Astrophysics 465 (April): 641–45. http://adsabs.harvard.edu/abs/2007A%26A...465..641G.

Gronoff, G., J. Lilensten, C. Simon, M. Barthélemy, F. Leblanc, and O. Dutuit. 2008. “Modelling the Venusian Airglow.” Astronomy and Astrophysics 482 (May): 1015–29. http://adsabs.harvard.edu/abs/2008A%26A...482.1015G.

Gronoff, G., J. Lilensten, L. Desorgher, and E. Flückiger. 2009a. “Ionization Processes in the Atmosphere of Titan. I. Ionization in the Whole Atmosphere.” Astronomy and Astrophysics 506 (November): 955–64. http://adsabs.harvard.edu/abs/2009A%26A...506..955G.

Gronoff, G., J. Lilensten, and R. Modolo. 2009b. “Ionization Processes in the Atmosphere of Titan. II. Electron Precipitation Along Magnetic Field Lines.” Astronomy and Astrophysics 506 (November): 965–70. http://adsabs.harvard.edu/abs/2009A%26A...506..965G.

Gronoff, G., C. Simon Wedlund, C. J. Mertens, and R. J. Lillis. 2012a. “Computing uncertainties in ionosphere-airglow models: I. Electron flux and species production uncertainties for Mars.” *Journal of Geophysical Research: Space Physics*, 117 (April): 4306, 18 PP., https://doi.org/10.1029/2011JA016930.

Gronoff, Guillaume, Cyril Simon Wedlund, Christopher J. Mertens, Mathieu Barthélemy, Robert J. Lillis, and Olivier Witasse. 2012b. “Computing Uncertainties in Ionosphere-Airglow Models: II. The Martian Airglow.” J. Geophys. Res. 117 (May): 17 PP. https://doi.org/201210.1029/2011JA017308.

Gronoff, G., Arras, P., Baraka, S., Bell, J. M., Cessateur, G., Cohen, O., Curry, S. M., Drake, J. J., Elrod, M., Erwin, J., Garcia-Sage, K., Garraffo, C., Glocer, A., Heavens, N. G., Lovato, K., Maggiolo, R., Parkinson, C. D., Simon Wedlund, C., Weimer, D. R., & Moore, W. B. (2020), Atmospheric Escape Processes and Planetary Atmospheric Evolution, Journal of Geophysical Research (Space Physics), 125(8), e27639, doi:10.1029/2019JA027639.

Kozelov, B. V., and V. E. Ivanov. 1992. "Monte Carlo calculation of proton-hydrogen atom transport in N_2." Plan. Space Sci. 40 (11): 1503–11. https://doi.org/10.1016/0032-0633(92)90047-R.

Kusakabe, Toshio, Kensuke Asahina, Jiang P. Gu, Gerhard Hirsch, Robert J. Buenker, Mineo Kimura, Hiroyuki Tawara, and Yohta Nakai. 2000. "Charge-transfer processes in collisions of H^+ ions with H_2, D_2, CO, and CO_2 molecules in the energy range 0.2-4.0 keV." Phys. Rev. A 62 (6): 062714. https://doi.org/10.1103/PhysRevA.62.062714.

Lilensten, J., P. L. Blelly, W. Kofman, and D. Alcaydé. 1999. "Auroral Ionospheric Conductivities: A Comparison Between Experiment and Modeling, and Theoretical F10.7-Dependent Model for EISCAT and ESR." Ann. Geophys. 14 (12): 1297–1304. https://doi.org/10.1007/s00585-996-1297-7.

Lummerzheim, D., and J. Lilensten. 1994. "Electron Transport and Energy Degradation in the Ionosphere: Evaluation of the Numerical Solution, Comparison with Laboratory Experiments and Auroral Observations." Annales Geophysicae 12 (November): 1039–51. http://adsabs.harvard.edu/abs/1994AnGeo..12.1039L.

McNeal, R. J. 1970. "Production of Positive Ions and Electrons in Collisions of 1-25-keV Protons and Hydrogen Atoms with CO, CO_2, CH_4, and NH_3." J. Chem. Phys. 53 (11): 4308–13. https://doi.org/10.1063/1.1673938.

Nakai, Y., T. Shirai, T. Tabata, and R. Ito. 1987. "Cross Sections for Charge Transfer of Hydrogen Atoms and Ions Colliding with Gaseous Atoms and Molecules." Atomic Data and Nuclear Data Tables 37 (January): 69. https://doi.org/10.1016/0092-640X(87)90005-2.

Nicholson, William P., Guillaume Gronoff, Jean Lilensten, Alan D. Aylward, and Cyril Simon. 2009. "A Fast Computation of the Secondary Ion Production in the Ionosphere of Mars." Monthly Notices of the Royal Astronomical Society 400 (November): 369–82. http://adsabs.harvard.edu/abs/2009MNRAS.400..369N.

Rudd, M. E., T. V. Goffe, R. D. Dubois, L. H. Toburen, and C. A. Ratcliffe. 1983. "Cross sections for ionization of gases by 5-4000-keV protons and for electron capture by 5-150-keV protons." Phys. Rev. A 28 (6): 3244–57. https://doi.org/10.1103/PhysRevA.28.3244.

Simon, C., J. Lilensten, J. Moen, J. M. Holmes, Y. Ogawa, K. Oksavik, and W. F. Denig. 2007. "TRANS4: a new coupled electron/proton transport code - comparison to observations above Svalbard using ESR, DMSP and optical measurements." Annales Geophysicae 25 (March): 661–73. https://doi.org/10.5194/angeo-25-661-2007.

Simon, C., O. Witasse, F. Leblanc, G. Gronoff, and J.-L. Bertaux. 2009. “Dayglow on Mars: Kinetic Modelling with SPICAM UV Limb Data.” Planetary and Space Science 57 (July): 1008–21. http://adsabs.harvard.edu/abs/2009P%26SS...57.1008S.

Simon, Cyril. 2006. “Contribution à L’étude Des Entrées d’énergie Solaire Dans L’ionosphère : Ions Doublement Chargés et Transport Cinétique Des Protons - Application à La Terre et à Titan.” PhD thesis, Université Joseph-Fourier - Grenoble I. http://tel.archives-ouvertes.fr/tel-00109802.

Simon Wedlund, C., G. Gronoff, J. Lilensten, H. Ménager, and M. Barthélemy. 2011. “Comprehensive calculation of the energy per ion pair or W values for five major planetary upper atmospheres.” Annales Geophysicae 29 (January): 187–95. https://doi.org/10.5194/angeo-29-187-2011.

Smith, K. A., M. D. Duncan, M. W. Geis, and R. D. Rundel. 1976. “Measurement of electron loss cross sections for 0.25- to 5-keV hydrogen atoms in atmospheric gases.” J. Geophys. Res. 81 (13): 2231. https://doi.org/10.1029/JA081i013p02231.

Toburen, L. H., M. Y. Nakai, and R. A. Langley. 1968. “Measurement of High-Energy Charge-Transfer Cross Sections for Incident Protons and Atomic Hydrogen in Various Gases.” Physical Review 171 (1): 114–22. https://doi.org/10.1103/PhysRev.171.114.

Werbowy, S., and B. Pranszke. 2016. “Charge-exchange processes in collisions of H^+,H_2^+,H_3^+,He^+ , and He_2^+ ions with CO and CO_2 molecules at energies below 1000 eV.” Phys. Rev. A 93 (2): 022713. https://doi.org/10.1103/PhysRevA.93.022713.

Witasse, O., O. Dutuit, J. Lilensten, R. Thissen, J. Zabka, C. Alcaraz, P.-L. Blelly, *et al.*, 2002. “Prediction of a CO22+ Layer in the Atmosphere of Mars.” Geophysical Research Letters 29 (April): 104–1. http://adsabs.harvard.edu/abs/2002GeoRL..29h.104W.

Witasse, O., O. Dutuit, J. Lilensten, R. Thissen, J. Zabka, C. Alcaraz, P.-L. Blelly, *et al.*, 2003. “Correction to ‘Prediction of a CO22+ Layer in the Atmosphere of Mars’.” Geophysical Research Letters 30 (April): 12–11. http://adsabs.harvard.edu/abs/2003GeoRL..30g..12W.

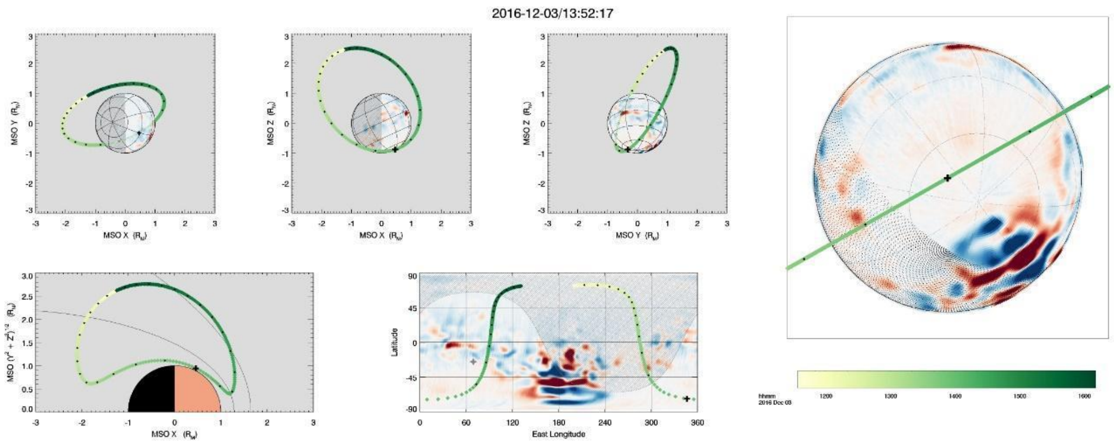

Figure S1. MAVEN spacecraft orbit information showing the locations of the spacecraft during Orbit 4235. The red/blue colors represent the magnitude and orientation of the crustal magnetic fields (see MAVEN PDS or Science Data Center website for more information). Note that the location of the periapsis is in the southern hemisphere and does not pass over any strong crustal magnetic fields.

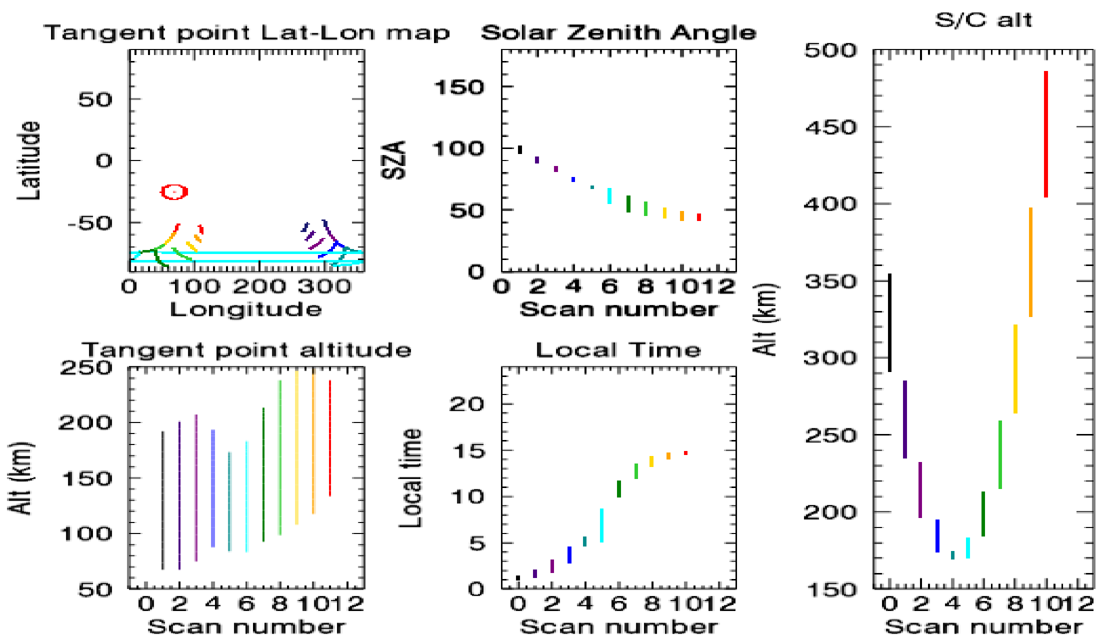

Figure S2. MAVEN/IUVS information showing ephemeris data for the IUVS limb scans during Orbit #4235 periapsis. Note that the location of periapsis is primarily on the dayside of the planet (with the exception of a few limb scan observations near the terminator) in the southern hemisphere and does not pass over any strong crustal magnetic fields. Different limb scans are marked by different colors within the orbit.

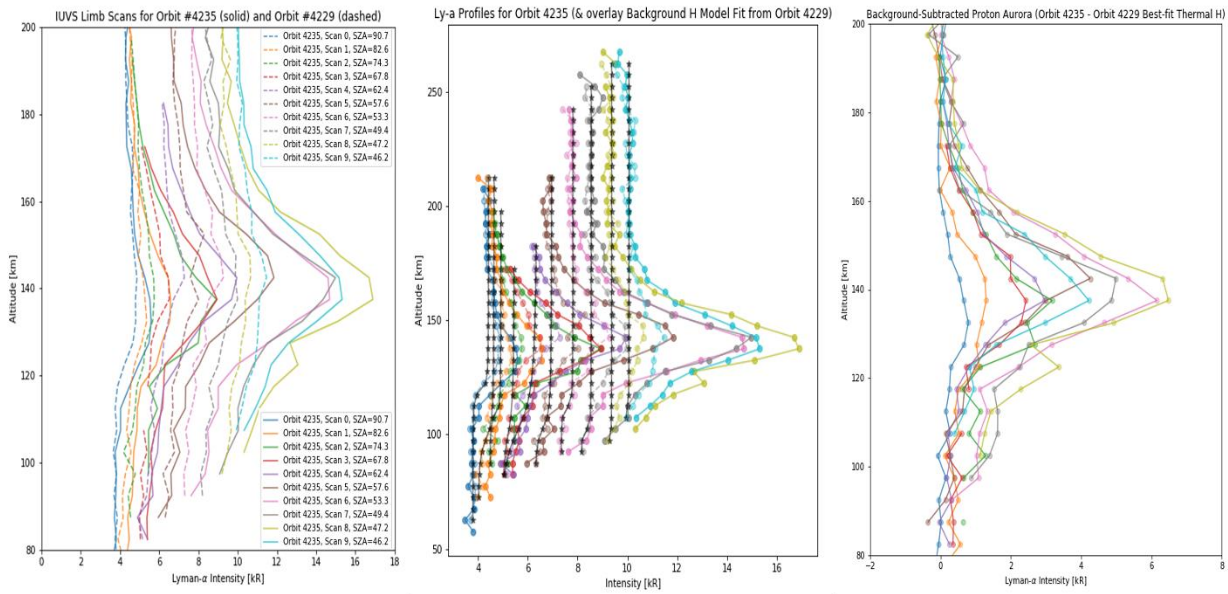

Figure S3. Altitude-intensity profiles and estimated heuristic thermal H background used for the background subtraction method described in this study. **Left**: IUVS Ly-α profiles for the orbit used in the data-model comparison (#4235), and a nearby orbit with little/less proton aurora activity (#4229) used to create the best-fit heuristic background coronal H profiles for each limb scan; peak profile SZAs for each scan in the two orbits are provided in the legend. **Middle**: Heuristic background thermal H profiles estimated from orbit #4229 (black profiles) overlain on Ly-α profiles for corresponding SZA limb scans in orbit #4235. **Right**: Final background-subtracted profiles that represent the contribution from only H-ENAs in the IUVS proton aurora observation in this orbit (*i.e.*, removing the background contribution from coronal thermal H).

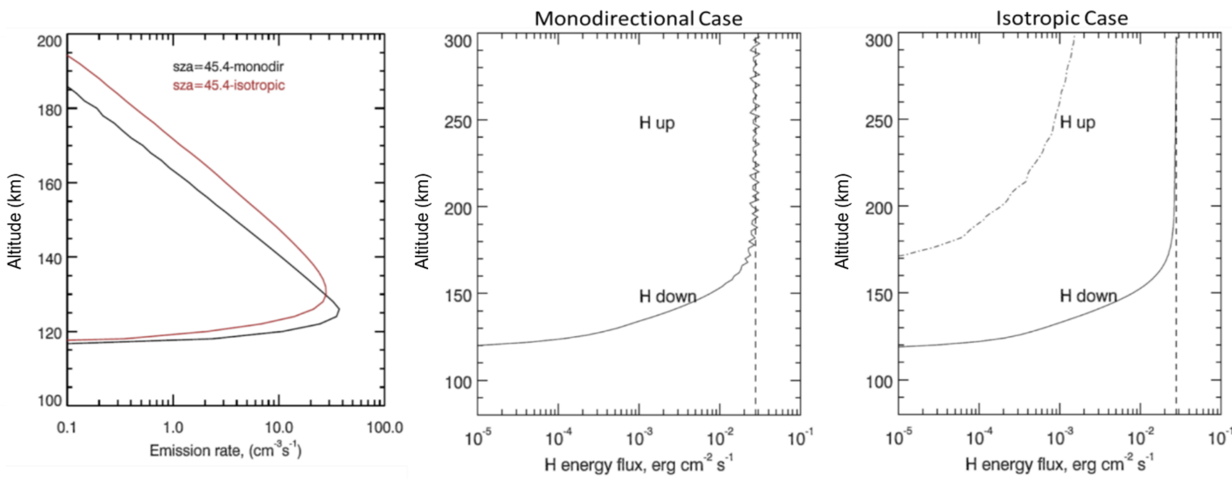

Figure S4. Example comparison of assuming monodirectional movement of the incident particle population in the atmosphere versus isotropic (simulation results from the Bisikalo/Shematovich *et al*. model). **Left:** Comparison proton aurora profiles using each assumption; **Middle:** Simulated H energy flux in the downward and upward (zero in this case) directions using a monodirectional assumption; **Right:** Simulated H energy flux in the downward and upward directions using an isotropic assumption. The simulated proton aurora profile using the isotropic assumption has a higher peak altitude and smaller VER due to the larger upward H population. The models in this study assume monodirectional particle movement, which could in turn lead to some of the observed discrepancies between the data and the models in Step 2 of the campaign. We note that neither of these two extreme assumptions (*i.e*., purely monodirectional or purely isotropic incident particle movement) is a probable physical occurrence, and the actual particle precipitation pattern is somewhere between these two limiting cases.

Cross Section (CS) Processes:	Elastic		Charge Exchange/ e^- Capture		e^- Stripping		Ionization		Lyman-α		Lyman-β &/or Lyman-γ		Balmer-α		Excitation of CO_2		Differential Scattering Cross Sections (DSCS)	
	$H-CO_2$	H^+-CO_2	$H-CO_2$	H^+-CO_2	$H-CO_2$	H^+-CO_2	$H-CO_2$	H^+-CO_2	$H-CO_2$	H^+-CO_2	$H-CO_2$	H^+-CO_2	$H-CO_2$	H^+-CO_2	$H-CO_2$	H^+-CO_2	$H-CO_2$	H^+-CO_2
Jolitz:	Newman+ 1986 [for $H/H^+ - N_2$]			Barnett+ 1977	Nakai+ 1987		Van Zyl+, 1978 [for $H - O_2$] McNeal, 1970 [rescaling]	Rudd+ 1985	Van Zyl & Neumann [for $H - O_2$] Birely & McNeal, 1971 [rescaling]	Avakyan+ 1998 [for $H^+ - O_2$] Birely & McNeal, 1971 [rescaling]			x	x			Newman+ 1986 Noel and Prölss, 1993 [for $H/H^+ - O_2$]	
Kallio:	Newman+ 1986 [for $H/H^+ - N_2$]			Rees, 1989 [for $H^+ - O_2$]	Van Zyl+, 1978 [for $H - O_2$]		Van Zyl+, 1978 [for $H - O_2$]	Rudd+ 1985	Van Zyl & Neumann, 1988 [for $H/H^+ - O_2$]				x	x			Newman+ 1986 Noel and Prölss, 1993 [for $H/H^+ - O_2$]	
Bisikalo/ Shematovich *et al.*:	Porter+ 1976			Nakai+ 1987 [for $H - O_2$ and rescaled]	Nakai+ 1987 [for $H - O_2$ and rescaled]		Haider+ 2002 [for $H - O_2$ and rescaled]		Haider+ 2002 [for $H - O_2$ and rescaled]				x	x			Lindsay+ 2005 [for $H/H^+ - O_2$ and rescaled]	
Gronoff *et al.*:	Kozelov & Ivanov, 1992 [for $H/H^+ - N_2$]			Kusakabe+ 2000 Avakyan+ 1998	Smith+ 1976 Avakyan+ 1998 [for $H - N_2$]		Basu+ 1987 [for $H - N_2$] Avakyan+ 1998 [rescaling]	Rudd+ 1983 Avakyan+ 1998	Birely & McNeal, 1972 [rescaled as per Avakyan+ 1998]		x	x			x	x	Avakyan+ 1998 Basu+ 1987 [Calculated from pitch angle using Rutherford-type collision functions]	

Table S1. List of cross sections (CS) that each model in this study may include. The five overlapping CS processes of each modeling team are shown in green, along with relevant references for those CS processes and Differential Scattering Cross Sections (DSCS). Bins marked with an "X" represent additional CS processes that can be included in models.